OFFICIAL USE ONLY

1. INTRODUCTION

The events of 11 September 2001 have caused most government organizations, departments, and agencies to examine the vulnerabilities to terrorist attack of the activities that they conduct or regulate. The U.S. Nuclear Regulatory Commission responded to concerns about terrorist attacks on nuclear fuel cycle facilities and activities by initiating a number of studies. This report presents the results of a study of jetliner crash into power reactor spent fuel transportation and storage casks.

1.1 Casks.

The study examined the crash of a large jetliner into a typical spent fuel transportation cask and a typical spent fuel storage cask. The transportation cask is a second generation steel-lead-steel rail cask that can carry a larger quantity of spent fuel than most other spent fuel rail casks. The storage cask examined was selected because it is likely to be widely used. Table 1.1 presents the dimensions and materials of construction used in these two casks.

Table 1.1. Cask Data

	Trasnportation Cask	Storage Cask
Spent Fuel		
Type Examined	PWR	PWR
No. Assemblies	24	24
Weight		
Canister		
Material	Steel	Steel
Wall Thickness		
Closure	Welded	Welded
Weight		
Overpack		
Length		
Materials	Steel-Lead-Steel	Steel-Concrete-Steel
Layer Diameters		
Layer Thicknesses		
Closure Seals	1 metal, 1 elastomer	
Closure Bolts		
Weight		
Impact Limiters		
Energy Absorbing Material	Wood	Aluminum honeycomb
Weight (each)		
Cask Loaded Total Weight		

1.2 Jetliner Crash Scenarios.

D/8

The crash of a larger passenger jetliner into a spent fuel transportation or storage cask might cause radioactive materials to escape from the cask to the environment. For the typical transportation cask examined by this study, this can happen only if some of the spent fuel rods, the cask canister, and the cask overpack all are breached. Because the concrete overpack of the storage cask is ventilated, release of radioactive materials from this cask can happen if some of the spent fuel rods fail and the canister is breached.

Crash of a jetliner into either of these casks could lead to breach of spent fuel rods, the cask canister, and/or the cask overpack in three ways. First, a major metal component of the jetliner, for example, the strut of the jetliner's front landing gear, could be driven through the cask overpack, the canister shell, and some of the spent fuel rods. Second, the impact of the jetliner onto the cask might launch the cask into some other very hard object, for example, another of the casks stored at the interim storage site, causing any of the barriers not failed by the initial jetliner impact to be failed by the second impact. Third, if enough jet fuel escapes the brief intense fireball characteristic of severe jetliner crashes, the resulting fuel pool fire could subject the cask to thermal loads that could fail any unfailed barriers, thereby allowing radioactive materials to be released to the environment.

1.3 Analysis Methods.

Analysis of the response of complicated structures to severe mechanical or thermal loads is done using large computer codes running on modern parallel processing computers. For this study, cask impact damage was analyzed using the CTH [1-1] and PRONTO [1-2] codes, the heat loads on the cask caused by pool fires were analyzed using the VULCAN fire code [1-3], and the response of the cask to these heat loads was analyzed using heat transport correlations. PRONTO, is a SNL developed transient-dynamic finite element code (similar in scope to DYNA-3D) that can analyze large deformations of highly nonlinear materials subjected to high strain rates. CTH is an Eulerian shock code developed at SNL to solve large deformation, strong shock wave, solid mechanics problems. Vulcan is a CFD code designed to solve turbulent reactive flow problems. The code handles gas dispersion and fire development scenarios with a variety of geometric constraints and boundary conditions.

Although the CTH and PRONTO analyses suggested that a jetliner crash into either of the two casks examined probably will not lead to cask failure, if either cask were failed by the impact and/or thermal loads caused by a jetliner crash into the cask, fission product release and the radiological consequences of the release would need to be modeled. Fission product release from these casks takes place in two steps, release of fission products from failed spent fuel rods into the canister, and transport of fission products through the canister to the environment. Because it implements a full suite of fission product transport models, fission product transport through the canisters of the two casks examined by this study can be modeled using the MELCOR thermal-hydraulic compartment code [1-4]. This code can also model release of fission products from spent fuel when that release is thermally driven. When release is driven solely by depressurization of failed fuel rods, which causes materials entrained in the depressurization flow of helium to be carried from the failed rods into the canister interior, release can be estimated using the methods developed for a recent reexamination of spent fuel transportation risks [1-5].

Once a radioactive source term to the environment has been estimated, radiological consequences can be estimated using the MACCS2 code [1-6] for sabotage events perpetrated at a specific location or the RADTRAN 5 code [1-7] for events perpetrated at some location along a transportation route. Because the MACCS2 code's plume rise model can not properly treat the buoyant rise of a pool fire plume, a pool fire plume rise model [1-8] was added to the MACCS2 code and its performance was validated. Finally, recent clean-up cost data was reviewed to determine if the clean-up cost estimates in the review of decontamination methods and costs performed by Chanin and Murfin [1-9] needed to be updated.

1.4 Roadmap

Section 2 of this report describes the CTH calculations performed to understand the damage done by jetliner impact into the transportation cask or the storage cask examined by this study, and also how the jetliner is damaged by impacting the cask. Section 2 also describes the damage done to these casks and the canister and spent fuel carried in the casks by impact of a simple model of a landing gear strut onto the shell or lid of the cask overpack. Section 3 describes the modeling of jet fuel fires, the thermal loads that a cask might be exposed to by jet fuel fires, and the response of the cask to those loads. Section 4 describes the MELCOR, MACCS2, and RADTRAN work performed to support analysis of fission product release from spent fuel transportation and casks and the consequences the release might cause should the impact and fire calculations indicate that release might be caused by a jetliner crash into either cask. Finally, Section 5 summarizes the threat posed by the crash of a jetliner into a spent fuel transportation or storage cask.

1.5 References

[1-1] R. L. Bell et al., "CTH User's Manual and Input Instructions, Version 6.0", Sandia National Laboratories, Albuquerque, NM, November 2000.

[1-2] L.M. Taylor and D. P. Flanagan, "PRONTO 3D A Three-Dimensional Transient Solid Dynamics Program," SAND87-1912, Sandia National Laboratories, Albuquerque, NM, March 1989.

[1-3] J. K. Holen and B.E. Vembe, "Benchmark cases calculated with Vulcan 97", Internal Department Report.

[1-4] R. O. Gauntt, R. K. Cole, et al., "MELCOR Computer Code Manuals, Version 1.8.5," NUREG/CR-6119, Rev 2. Office of Nuclear Regulatory Research, U.S. Nuclear Regulatory Commission. Washington, DC, 2000.

[1-5] J. L. Sprung et al., "Reexamination of Spent Fuel Shipment Risk Estimates," NUREG/CR-6672, U.S. Nuclear Regulatory Commission, Washington, DC, March 2000 (URL: ttd.sandia.gov/nrc/modal.htm).

[1-6] D. I. Chanin and M. L. Young, "Code Manual for MACCS2: Volume 1, User's Guide", SAND97-0594, Sandia National Laboratories, Albuquerque, NM, March 1997.

[1-7] K. S. Neuhauser, R. F. Weiner, and F. L. Kanipe, "RADTRAN 5, Technical Manual," SAND2000-1256, Sandia National Laboratories, Albuquerque, NM , June 2000 (available on the RADTRAN web site).

[1-8] M. T. Mills, Modeling the Release and Dispersion of Toxic Combustion Products from Chemical Fires, Presented at the International Conference on Vapor Cloud Modeling, 11/1987, Cambridge MA.

[1-9] D. I. Chanin and W. B. Murfin, "Site Restoration: Estimation of Attributable Costs from Plutonium-Dispersal Accidents," SAND96-0957, Sandia National Laboratories, Albuquerque, NM, May 1996.

4. Source Terms and Consequences

4.1 Introduction

If a jetliner impact onto a spent fuel transport or storage cask caused all barriers to fission product release (the spent fuel rods, the cask canister, and for transportation casks the cask overpack) to fail, the source term released to the environment and the radiological consequences caused by that release would need to be estimated. This can be done as follows:

- Calculate the radioactive inventory of the cask.
- Estimate the fraction of the rods in the cask that are failed by the sabotage event.
- Estimate the fraction of the radioactive materials in a failed rod that escape from the rod into the cask's canister.
- Estimate the fraction of these materials that transport through the canister to the canister leak without depositing onto canister interior surfaces, through the leak into the cask overpack, and through the cask overpack to the environment.
- Perform consequence calculations that estimate downwind transport of the released radioactive materials, contamination of land and property, radiation doses and radiation induced health effects among the exposed population, and economic costs.

Rod Failure Fractions. Spent fuel rod cladding will fail if subjected to strains that exceed the strain failure criterion for Zircaloy metal. The cladding will also fail if it is heated to burst rupture temperatures. NUREG/CR-6672 [4-1] presents an analysis of both of these failure mechanisms. NUREG/CR-6672 estimated rod failure fractions caused by cask impacts by scaling a 30 mph rod strain map [4-2] to higher impact speeds using the peak acceleration in the cask shell as the scale factor and comparing the scaled strain map to a rod strain failure criterion that varied with fuel burn-up. All rods with scaled strains that exceeded the strain failure criterion anywhere along their length were assumed to fail. For failure by burst rupture, NUREG/CR-6672 assumed that any rod heated to 750 °C would fail by bursting.

Release of Radioactive Materials from Failed Rods. A critical review of the mechanisms of release of radioactive materials from failed spent fuel rods was performed for the NUREG/CR-6672 study [4-1]. The following paragraphs summarize the release models developed by this review for Noble Gases, Particles, compounds of Cesium and Ruthenium, and CRUD (activated deposits on rod outer surfaces that can be released by spallation, if the rod is subjected to mechanical or thermal loads).

Noble Gases. PWR spent fuel rods are pressurized with helium to about 30 atmospheres and BWR rods to about 15 atmospheres. Thus, when a spent fuel rod fails and depressurizes to atmospheric pressure, almost all of the gasborne species will be carried out of the rod with the depressurization flow of helium. Thus, if the occlusion of noble gas atoms in fuel fines is unimportant or neglected, rod-to-cask release fractions for noble gas fission products should have values close to 1.0.

Particles. In order to develop particle release fractions that apply to transportation accidents, the release fraction for fuel fines determined by Lorenz [4-3] must be adjusted to account for impact fracturing caused by impact loads, particle bed formation, and filtering of respirable particles during transport through particle beds. The fraction of the UO_2 fuel mass converted to respirable fuel fines by pellet fracturing due to impact loads during collision accidents was modeled [4-4] as $F_{respirable} = A\rho gh = 0.5\ A\rho(v_{impact})^2$. Because the dependence of A on v_{impact} was not available, v_{impact} was assumed to be 120 mph for all collisions even though collapse of assembly structures is expected to absorb much of the energy associated with the cask impact. Impact fracture data for depleted UO_2 shows [4-5] that 99 percent of the total particle mass is in particles with diameters ≥ 200 μm. Because the internal cracks in spent fuel pellets and the shrunken fuel cladding gap in spent fuel rods have widths much smaller than 200 μm, fuel fine particle beds should form in these spaces and be augmented by fuel fracturing during collision accidents. Interception will be the dominant particle capture mechanism by a bed of 200 μm particles [4-6]. If the total bed capture efficiency is equated to the interception efficiency, solution of the resulting equation shows that bed lengths of about 0.3 cm will collect 99 percent of the 10 μm particles that pass through the bed. Accordingly, for collision accidents, efficient filtering was assumed to occur along almost the entire length of the rod. For fire-only accidents, the release fraction for particles determined by Lorenz by examination of 1 ft sections of spent fuel rods was applied to the 1 ft portion of the full rod that contains the rod failure and particle bed formation and efficient filtering was assumed to apply to the remaining 11 feet of active fuel.

Cesium. Although the equation for release of Cs determined by Lorenz et al. [4-7, 4-8] has the form A exp (– C/T) and thus has the form of a vapor pressure equation, the experimental value of C, 7420 K^{-1}, it not similar to the value of C for any reasonable Cs vapor species. For example, the value of C for CsI, when the vapor pressure equation for CsI is expressed as an exponential, is 22862 K^{-1}, not 7420 K^{-1}. This discrepancy is explained as follows. Lorenz et al. measured total Cs, not Cs in vapor species. Since their experiments released Cs as a constituent, not only of vapors, but also of particles, Cs release should have been modeled as the sum of a particle release expression and a vapor release expression. If the Cs release expression of Lorenz et al. is equated to the sum of a release fraction for CsI vapor and a release fraction for particles, the following equation is obtained:

$$\alpha V_{burst}\left(\frac{M_{gap}}{A_{clad}}\right)^{0.8}\exp\left[-\left(\frac{C}{T_b}\right)\right] = MW_{CsI}\frac{V_{rod}}{RT_b}10^{-a/T_b+b} + M_{inventory}F_{particles}$$

Substitution of CsI values for MW_{CsI} and for a and b [4-9] and values developed by Lorenz et al. [4-7, 4-8] for all other parameters in this expression except C, allows a value of C = 7960 K-1 to be calculated. Since this agrees well with the experimental value determined by Lorenz et al., Cs release was assumed to occur both as CsI (or CsOH) vapor and was modeled using the two terms on the right side of the preceding equation.

Oxidative Release Fractions. The double cask failure assumed for Category 6 accidents allows combustion gases and air to flow through the cask. This flow was assumed to have two effects. First, it was assumed to transport out to the environment all materials released from failed rods to the cask interior (i.e., for Category 6 accidents, deposition of particles and vapors onto cask interior surfaces was neglected). Second, the O_2 and CO_2 in this gas flow was assumed to

oxidize any exposed fuel pellet surfaces. Lorenz et al. [4-3] found that Cs release and Ru release were increased respectively by factors of 54.6 and 2.02×10^4 when the experimental atmosphere was dry air rather than steam. The increase is believed to be caused by the oxidation of involatile RuO_2 to volatile RuO_4 and of UO_2 to U_3O_8, which increases the pellet surface area and facilitates the escape of Cs vapors. If, as is shown in Figure 3, this oxidation is assumed to occur in a small disc of UO_2 with a height h_{ox} and a volume V_{ox}, that is located below the burst rupture failure hole in the rod section, and, in addition, release of Cs and Ru from this oxidized disc is assumed to be total, then use of either the Cs or the Ru enhancement factor allows the height of this disc to be estimated to be about 0.1 mm and its volume to be 0.3 mm^3. Therefore, the ratio of the oxidized volume of spent fuel in a failed rod to the volume of all of the pellets in that rod gives the release for Cs and Ru, that is caused by oxidation of spent fuel, when that fuel is exposed to oxygen at temperatures $\geq T_b$, the burst rupture temperature of spent fuel rods.

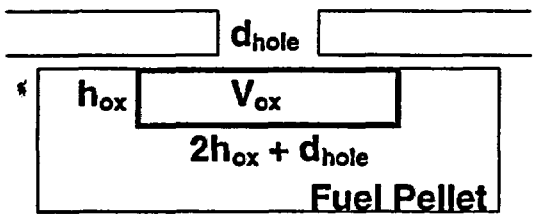

Figure 3. Schematic of Oxidized Spent Fuel Disc

CRUD. Reactor water chemistry causes deposits that contain Ni to form on the surface of spent fuel rods. Activation of Ni then produces Co-60, which can be released if these CRUD deposits spall off of rod surfaces due to mechanical or thermal loads during transportation accidents. There is almost no data on CRUD spallation. Sandoval et al. [4-10] estimated that CRUD spallation might cause 15 percent of the CRUD deposits on a spent fuel rod to be released during transportation accidents. In the absence of additional data, the NUREG/CR-6672 study assumed that spalled CRUD would deposit onto cask interior surfaces like fuel fines (e.g., same deposition fractions) and that the fraction of the CRUD deposits on rod surfaces released by spallation would be 0.1 for collision accidents, 0.05 for fires initiated by collisions, and 0.15 for fires not initiated by collisions.

Transport of Radioactive Materials Through the Canister. Transport through the canister of radioactive materials released from failed rods into the canister can be modeled using the MELCOR [4-11] compartment code, which can model any structure that can be represented by a set of irregular volumes connected by flow paths. Because MELCOR implements a full suite of thermal, hydraulic, and fission product transport models, it can model fluid flow (e.g., gases, liquids) through and between compartments, fission product transport with these fluid flows, and condensation and evaporation of fission product vapors and deposition of particles onto compartment surfaces. In addition, MELCOR can model the thermal release of fission products from spent fuel pellets using simple Arrhenius rate expressions.

A MELCOR model of an undamaged storage cask system (overpack, canister, baskets, and fuel assemblies) was developed for the NRC by a previous SNL study. A MELCOR model of an undamaged transportation cask system was developed for this study. The sensitivity of fission product release to the cross-sectional area of the canister leak path has been performed using both models. In addition, enhancement of release by the oxidation of Zircaloy cladding by

exposure to air while at moderately elevated temperatures was examined for the storage cask system. Section 4.2 describes the results of these MELCOR analyses.

Consequence Calculations. The ground contamination levels, radiation doses, and health effects caused by a release of radioactive materials to the atmosphere are calculated using either a site specific consequence code, for example MACCS2 [4-12], if the accident location is known, or a transportation accident consequence code, for example RADTRAN 5 [4-13, 4-14], if the accident might occur anywhere along the length of a radioactive material shipment route.

Consequence codes typically calculate

- downwind transport of the released radioactive materials as a function of the prevailing atmospheric conditions at the time of the accident,
- deposition of radioactive materials onto the ground by washout and gravitational settling,
- exposure of people to radiation by the following five exposure pathways: cloudshine, inhalation of plume materials, groundshine from deposited radionuclides, inhalation of radioactive materials resuspended from the ground, and ingestion of radioactive materials by consumption of contaminated water or foods,
- mitigation of these exposures by emergency response (evacuation, sheltering) and also by post-accident recovery actions (decontamination or condemnation of contaminated property), and
- the health effects (acute morbidity and fatalites; radiaction induced cancers and cancer fatalities, genetic effects) caused by these exposures.

Both MACCS2 and RADTRAN 5 use simple Gaussian plume models to estimate downwind transport of airborne materials. MACCS2 performs this calculation internally; RADTRAN performs the transport calculation for a unit release external to the code and then uses the resulting air and ground concentrations as code input data. Because simple Gaussian plume models do not treat the effects of building wakes and surface roughness on deposition, nearfield (yield < 500 m) ground concentrations are poorly predicted by either code. RADTRAN 5 assumes that all releases are cold and thus not subject to plume rise. MACCS2 contains a plume rise model for the release of a buoyant plume from a point source. Because jet fuel fires are an area source, the plume rise model in MACCS 2 was supplemented by implementing the Mills pool fire plume rise model [4-15] and validating its performance. The validation of this model is described in Section 4.3 below.

Both codes assume that fission products transport either as non-condensible gases (e.g., Xe) or as particles. Particle deposition to surfaces is modeled using a deposition velocity or a simple washout model. Radiation doses received by each exposure pathway modeled are calculated using dose conversion factors. Health effects are calculated using non-linear models for acute health effects and linear no-threshold models for cancer fatalities.

Both codes can estimate economic consequences. However the models are quite simple and better results can be obtained by performing hand calculations using the ground contamination

results from the consequence calculations and decontamination factors and cleanup costs taken from the literature that reflect the timing of the cleanup activities.

Because the weather data needed by consequence calculations can always be obtained from a nearby National Weather Service Station or from a local airport (e.g., a local windrose) and population data can be calculated using 2000 census data, only the cask inventory inventory and the release fractions that specify the amount of that inventory that is released by the accident need to be developed before a consequence calculation can be performed. The inventory is calculated using the ORIGEN code [4-16]. Rod-to-canister release fractions are developed using the NUREG/CR-6672 methodology and canister-to-environment release fractions are developed by MELCOR calculations.

Lastly, cleanup methods and their costs were critically reviewed by Chanin and Murfin in 1996 [4-17]. That review found that the effectiveness of decontamination methods was a very strong function of the length of the time period between the accident and the start of the cleanup. The longer the delay, the more tightly the deposited materials bind to the surfaces on which they deposited. In addition, because regulatory guidance for cleanup of radioactive contamination is sparse, the end of this time period is likely to be much delayed by litigation. Since these two effects very strongly influence cleanup cost estimates, a brief literature review was conducted to determine whether new information was available that would significantly alter the conclusions of Chanin and Murfin. The results of that review are discussed in Section 4.4 below.

4.2 MELCOR Calculations

If an analysis of a jetliner crash into a spent fuel storage or transportation cask were to predict the failure of at least some spent fuel rods, the cask canister, and for transportation casks the cask overpack, a fission product transport calculation would need to be performed to estimate the fraction of the cask inventory that escapes to the environment. For this study, the MELCOR code [4-11] was selected to perform fission product analyses. Because of the early completion date for the jetliner crash analyses, development of MELCOR input data was begun before the damage done to the transportation and storage casks being examined by this study had been determined.

4.2.1 Brief description of the MELCOR Code

The MELCOR code is a flexible, general-purpose simulation code that was originally intended for analysis of severe accidents in commercial light-water reactors. Throughout the years, MELCOR's versatility has been exploited, and analysts have simulated a wide myriad of systems including home heating and ventilation systems, pumps, aerosol behavior, containment response, blow down facilities, fuel casks, and of course, nuclear reactors.

MELCOR treats fluid flow and heat transfer, core heat-up, degradation, and relocation, fission product release and aerosol behavior, engineered safety features, ex-vessel phenomena, and control systems. In addition, MELCOR features source code modifications at the user-input level, and has flexible input.

In order to adequately model fuel casks, a code should calculate natural circulation, heat conduction, thermal radiation, Zircaloy and stainless-steel oxidation, fission product release, aerosol transport, and heat source input. These models already exist in MELCOR, thus making MELCOR a tool of choice for fuel cask analysis.

Transport through the canister of radioactive materials released into the canister from failed rods can be modeled using MELCOR, which can model any structure that can be represented by a set of volumes connected by flow paths. Because MELCOR implements a full suite of thermal, hydraulic, and fission product transport models, it can model fluid flow (e.g., gases, liquids) through and between compartments, fission product transport with these fluid flows, and condensation and evaporation of fission product vapors and deposition of particles onto compartment surfaces. In addition, MELCOR can model the thermal release of fission products from spent fuel pellets using simple Arrhenius rate expressions. In particular,

$$\dot{f} = f_o \exp\left(-\frac{Q}{RT}\right) \tag{1}$$

where

$\dot{f}$ = release rate (fraction/unit time)

f_o = function of fuel burnup

Q = activation energy

R = universal gas constant

T = temperature.

4.2.2 MELCOR Zircaloy Oxidation Kinetic Expressions

The MELCOR code contains a solid state and gaseous diffusion model for the oxidation of Zircaloy by oxygen and/or steam. The Zircaloy steam and oxygen oxidation reactions are exothermic, meaning that heat is released as the oxidation proceeds.

Solid-state diffusion of oxygen and/or steam through an oxide layer to unoxidized metal is represented by the parabolic rate equation

$$\frac{d(W^2)}{dt} = K(T) \tag{2}$$

where

W = mass of metal oxidized per unit surface area

K(T) = a rate constant expressed as an exponential function of surface temperature *T*.

and K(T) is also Arrhenius equation.

For the Zircaloy-steam oxidation reaction,

$$K(T) = 29.6 \exp\left[\frac{-16820.0}{T}\right] \quad \text{for } T < 1853.0\ \text{K} \tag{3}$$

$$K(T) = 87.9 \exp\left[\frac{-16610.0}{T}\right] \quad \text{for } T \geq 1853.0\ \text{K} \tag{4}$$

For very low oxidant concentrations, gaseous diffusion may limit the reaction rate. The oxidation rate when limited by gaseous diffusion is given by

$$\frac{dW}{dt} = \frac{MW\, k_c P_{ox}}{nRT_f} \tag{5}$$

where

MW = molecular weight of metal being oxidized
k_C = mass transfer coefficient
P_{ox} = partial pressure of oxidant (H_2O or O_2)
n = number of oxidant moles (H_2O or O_2) consumed per mole of metal
R = universal gas constant
T_f = gas film temperature = $(T + T_{gas})/2$

Note that the gaseous diffusion oxidation rate is used if it is less than the rate calculated by the solid-state diffusion equations.

4.2.3 MELCOR Cask Models

A MELCOR model of the storage cask being examined by the jetliner crash analyses had been previously developed by SNL for another NRC project. Construction of a model of the vulnerability study's transportation task being examined by the jetliner crash analyses was begun during the summer of 2002.

4.2.3.1 Spent Fuel Storage Cask

The storage cask system for dry storage of spent nuclear fuel modeled in this study consists of a loaded multipurpose canister (MPC) housed in a ventilated concrete over. The storage over-pack provides gamma and neutron shielding, air ducts for ventilation, missile protection, and protection against natural phenomena and hypothetical accidents involving the MPC. The MPC is a sealed canister that contains a honeycombed fuel basket which can carry 24 PWR spent fuel assemblies and 68 BWR assemblies. Figure 4.1 presents a view of a horizontal cross-section of the cask system that shows the shell of the concrete overpack, the shell of the MPC, and the honeycomb structure that houses the 68 BWR assemblies carried in the MPC. The vertically oriented cylindrical canister shells are welded to the canister's baseplate and lid, and the lid

isfitted with welded port cover plates and a closure ring. Dimensions for this cask system are given in Table 4.1.

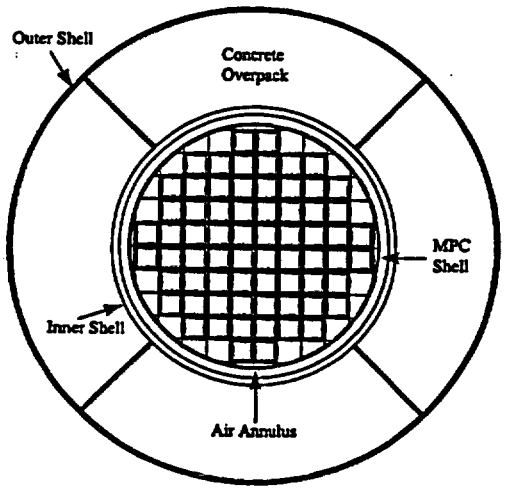

Figure 4.1. Spent fuel dry cask storage system

Table 4.1. Spent fuel storage cask system dimensions and MPC-68 physical parameters.

HI-STORM 100 component	Dimension	Physical parameters:	MPC-68
Over-pack length	5.8738 m	Max assembly width	0.1486 m
Over-pack lid OD	3.2004 m	Max assembly length	4.4755 m
Over-pack baseplate OD	3.4004 m	Max assembly weight	317.5 kg
MPC length	4.8387 m	Max active fuel length	3.81 m
MPC OD	1.7367 m	Fuel rod clad material	Zircaloy

4.2.3.2 Spent fuel storage cask MELCOR model

The MELCOR model of this spent fuel dry cask storage system consists of a collection of heat structures (HSs) and control volumes (CVs) that communicate by means of flow paths (FPs). The modified nodalization scheme used in this study is shown in Figure 4.2.

Figure 4.2 shows that the region housing the SNF is segmented into three equal area radial rings. These rings are divided axially into ten levels. The fueled region along with control volumes 121 and 122, representing the unfueled outer annular flow region of the MPC, and control volume 222, representing the open space under the upper cover plate, together with the connected flow paths provide the conduit for flow of the working thermal fluid, helium. Cooler ambient air enters through lower over-pack vents represented by FP398. The chimney effect

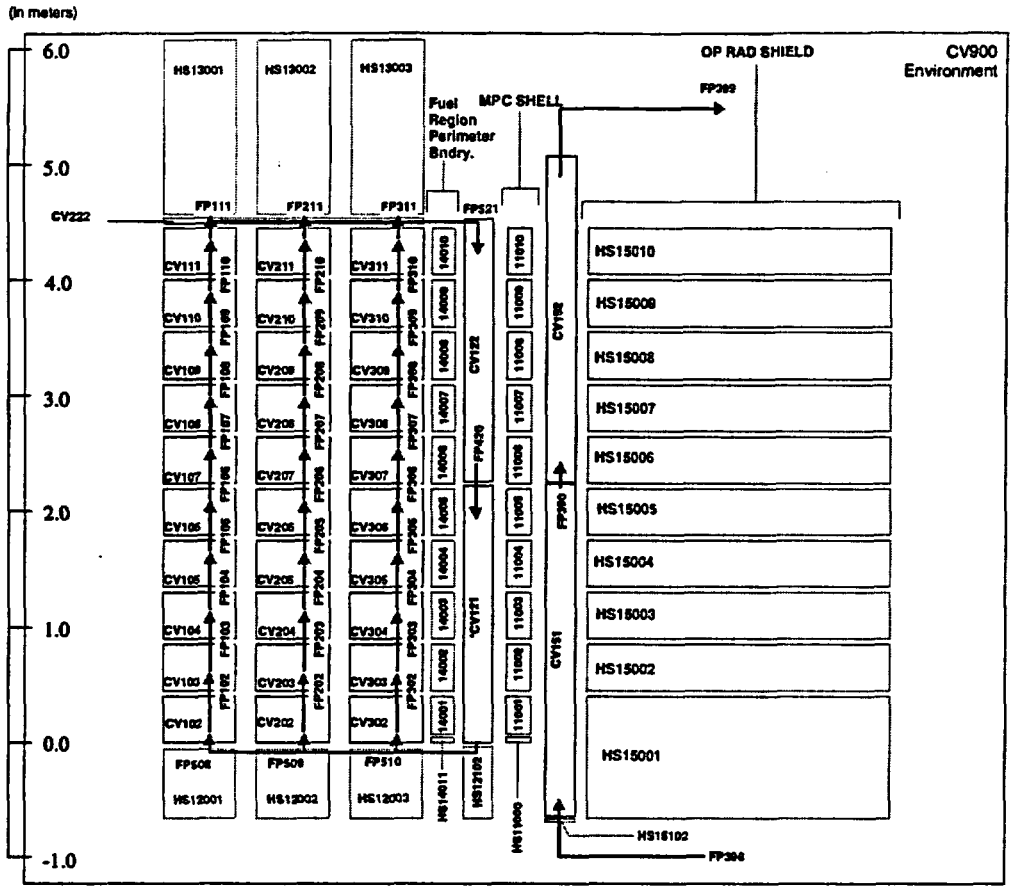

Figure 4.2. MELCOR model of the spent fuel storage cask.

induces circulation within the system thus providing passive heat convection through the over-pack vents. In essence, heat is transferred to air in the chimney via radiation and conduction through heat structures and then vented to the atmosphere through FP399. The flow path arrows in Figure 4.2 indicate the direction of natural circulation flows present in the MPC during normal operation. As shown in the nodalization diagram, the upper lid, lower platform, MPC shell, and over-pack are represented by heat structures. The fuel region perimeter boundary is represented by a heat structure that facilitates heat transfer from the fueled region to the MPC shell. The heavy-walled steel and concrete cylindrical over-pack is represented by the HS15000 series in the nodalization diagram.

To model core thermal radiation, exchange or view factors are used. Radiation view factors between the heat sinks are derived by approximating each heat sink as a separate flat plate. Thus, in a rudimentary sense, these view factors describe the geometric orientation between pairs of surfaces. The view factors account for radiative exchange from the canister wall to the fuel

rod cladding; radiation from "other structure" to the adjacent canister walls or to fuel rods and debris if the canister is not present; radiation radially outward from the cell boundary to the next adjacent cell; and radiation axially upward from the cell boundary to the next adjacent cell. All of these parameters (FCNCL, FSSCN, FCELR, FCELA, and FLPUP) are assigned the value of 0.1 in the model.

Reactor shutdown time is 1.5768×10^8 seconds (~ 5 years). In this case, it constitutes the time the fuel has been out of the reactor. Decay power of the nuclides (DCHDECPOW) is computed from the ANS standard calculation for whole core decay heat. Decay heat input was adjusted to attain a total of 22kW for the analysis in this report. All default classes listed in the DCH package in the MELCOR reference manual are used in the radionuclide calculation

Thermodynamic input characterizing the internal MPC environment included: pressure (PVOL = 2.9×10^5 Pa); atmospheric temperature (TATM = 300 K); partial pressure of water vapor in the atmosphere (PH2O = 0.0); and mole fraction of noncondensible gas n (MLFR.n), 100% helium environment. This reflects the initial fill conditions for the MPC prior to attaining a steady state temperature. Upon closure, the fuel will heat up and a higher fill pressure will result. For the over-pack, the thermodynamic input included: pressure (PVOL = 1.0×10^5 Pa); atmospheric temperature (TATM = 300 K) and dew point temperature (TDEW = 280.0 K). The mole fractions of non-condensible gases are 0.8 for nitrogen and 0.2 for oxygen, representative of the composition of air. Thermodynamic conditions are defined by tabular and control functions (i.e., ambient conditions in the environment external to HI-STORM).

4.2.3.3 Assessment of the MELCOR spent fuel storage cask model

Normal Operation. In the MELCOR model, under steady-state operating conditions, as Figure 4.3 shows,decay heat varied from about 22 kW to as low as 21.3 kW. This range is consistent with decay heat values reported in the TSAR and in the COBRA-SFS analysis of the Holtec HI-STORM 100 ventilated concrete cask storage system.

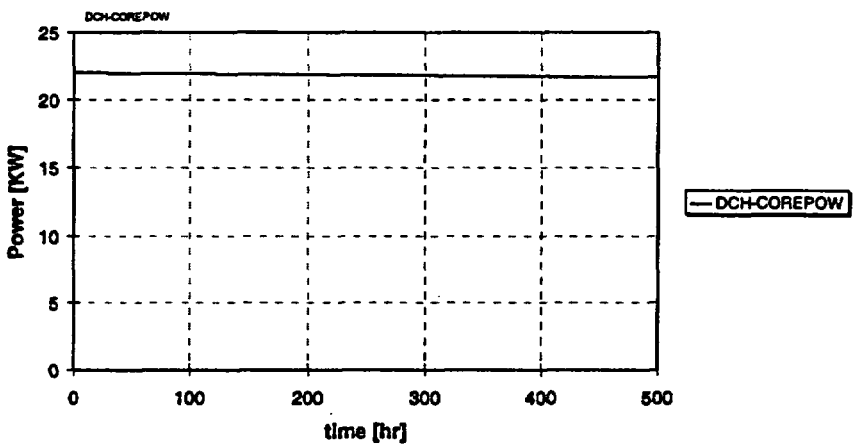

Figure 4.3. Decay power used in storage cask analysis.

Natural circulation within the MPC system develops as steady state conditions are attained as evidenced from the velocity profile shown in Figure 4.4.

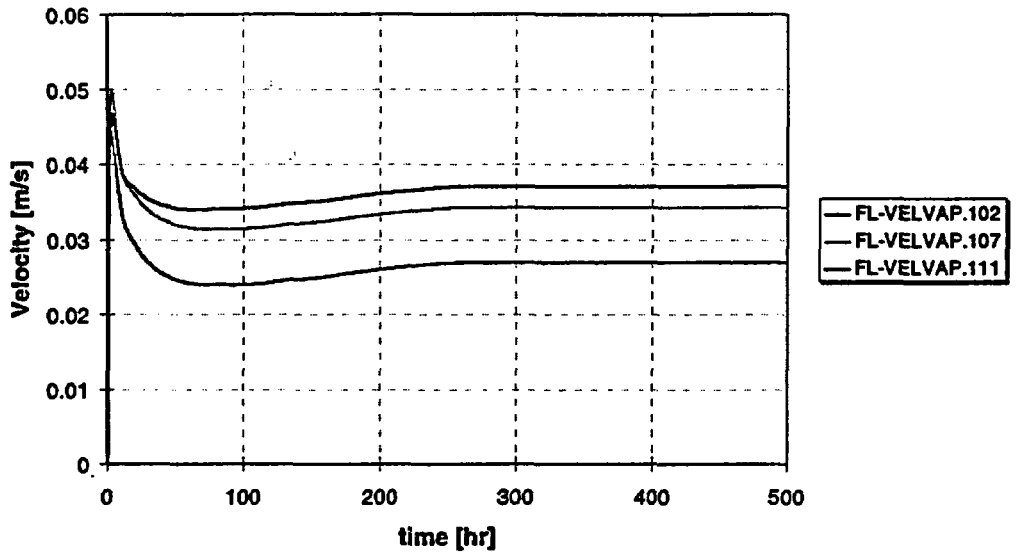

Figure 4.4 Velocity of rising helium gas in the central ring of the MPC.

Computed steady state velocities varied from 0.0297 m/s (0.0974 ft/s) at the bottom of the fueled region to 0.0364 m/s (0.1193 ft/s) exiting the fueled region. These velocities compare favorably with the Cobra-SFS output obtained from PNNL. COBRA-SFS velocity varied from 0.0333 m/s (0.1093 ft/s) at the bottom of the fueled region to 0.0501 m/s (0.1645 ft/s) exiting the fueled region. In the Cobra-SFS model, ambient temperature of 80°F, internal helium pressure of 5 atmospheres, and total decay heat of 21.5 kW were used. The Cobra-SFS model was run in steady state mode and yielded peak clad temperature of ~568.4K (563.5°F).

Initial system and component temperatures were 300K (~80°F) for this study. Fuel and heat structures slowly approach the steady state temperature distribution established by decay heat. Figure 4.5 shows the temperature distribution for the cladding of the central-most radial fuel ring as it approached equilibrium. Temperatures ranged from 496 to 623K (433 to 662°F). The clad temperature profile clearly displays the expected pattern, cooler temperatures at the bottom with temperatures increasing along the length as the buoyant helium gas transports the heat up the length of the region into the plenum by convection.

The initial system pressure of the helium filled MPC is 2.86 atmosphere. As depicted in Figure 4.6, after the steady state equilibration period is reached system pressure is on the order of 5.18 atmosphere.

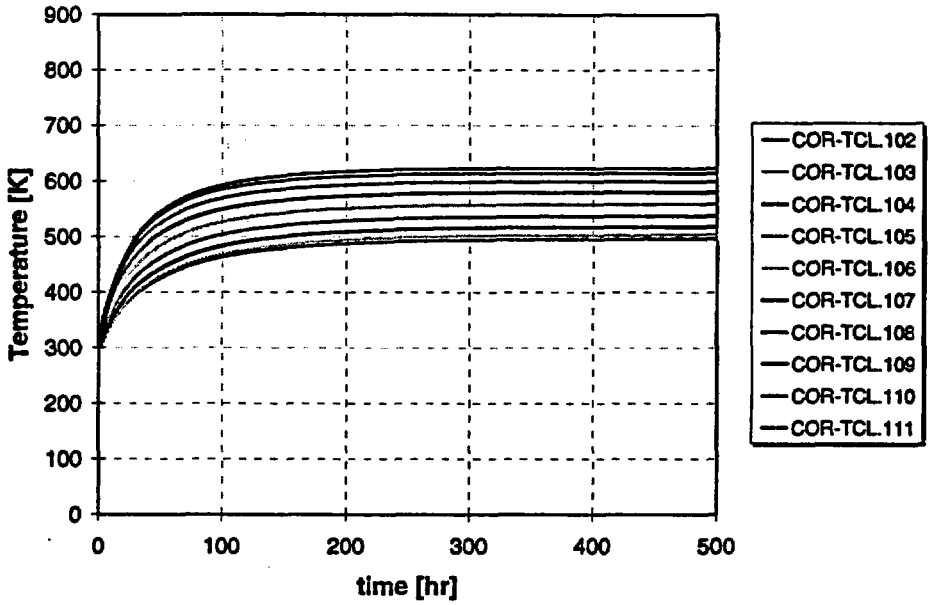

Figure 4.5. Ring 1 fuel clad temperatures as cask comes to equilibrium in normal operation.

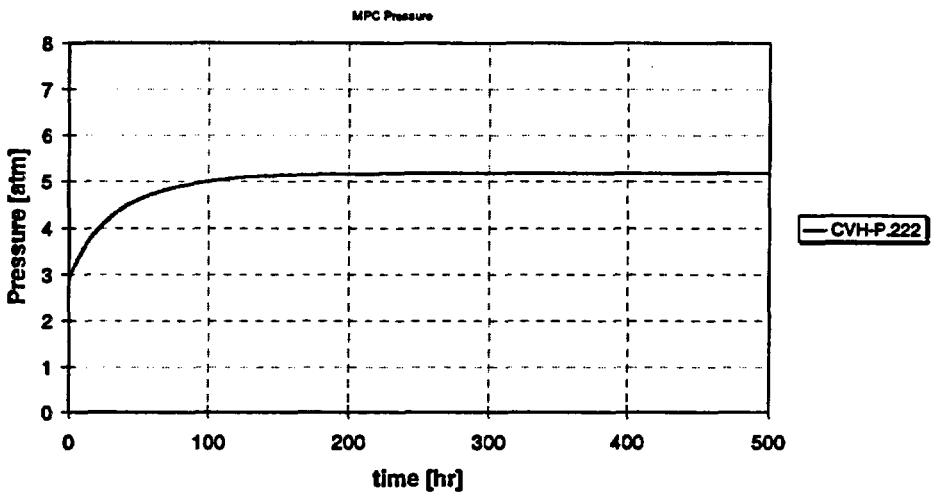

Figure 4.6. MPC pressure response at mid-height to normal operating conditions.

Maximum temperatures anticipated during normal storage for the this cask, canister, and with its MPC-68 basket were extracted from the TSAR. Table 4.2 compares these temperatures to the maximum temperatures obtained from the MELCOR calculation for normal operating conditions. Figure 4.7 displays the MPC and over-pack temperature response under normal operating conditions at mid-height.

Table 4.2. Maximum temperatures (normal operating conditions).

Component	Normal Condition Temp, K (°F)	MELCOR Model[‡] Temp, K
Fuel cladding	667.6 (742)	623
MPC outer shell	422.6 (301)	489
Concrete Over-pack inner shell	350.4 (171)	349
Concrete cross sectional average	339.3 (151)	-
Concrete over-pack outer shell	328.2 (131)	307
Over-pack lid bottom plate at centerline	357.0 (183)	482
Over-pack lid top plate	343.7 (159)	552
Air outlet	358.2 (185)	338

[‡]COR-TCL.111; HS1101001; HS1501011; n/a; HS1501034; HS12002; HS13002; and CVH-152

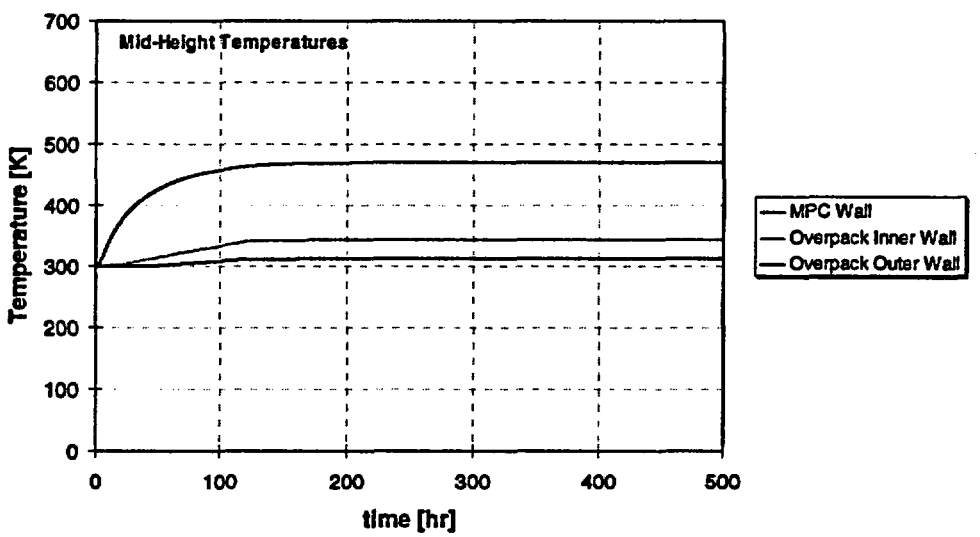

Figure 4.7. MPC and over-pack temperature response at mid-height to normal operating conditions.

The analyses presented in this section characterize the thermal response under normal operating conditions of the spent fuel storage cask system examined by the jetliner crash analyses and

show that the MELCOR results compare reasonably well with performance metrics presented in the TASR for this cask system. Accordingly, these steady state conditions are used as initial conditions for the various off-normal events analyzed in the following sections.

Off-normal cask response analysis. As Section 2 of this report shows, only a few large hard components of a jetliner appear able to fail the storage cask by impact. Moreover, because the impact of a hard jetliner component (e.g., the front landing gear strut) does not seem likely to fail most of the spent fuel rods in the cask, these jetliner crash scenarios may not lead to the release of large quantities of radioactive materials. Accordingly, only those sabotage scenarios that can lead to rod failure as a result of heating of the storage cask may be able to cause consequences of concern.

Jetliner crash scenarios that initiate jet fuel fires were considered in Section 3. The analysis presented in that section suggests that jetliner crash fuel fires with durations long enough to pose a problem seem unlikely. However, two unlikely scenarios might worsen the effects of fires. First, if cask failure allowed air ingress into the fuel assembiles, then the highly exothermic Zircaloy-oxygen reaction might be initiated. Second, if the cask were to be buried in rubble, then blocking of the cask vents could allow canister temperatures to rise possibly causing both spent fuel rods and the canister itself to fail. These two unlikely storage cask thermal scenarios were examined by performing MELCOR calculations.

Air ingression and Zircaloy air oxidation. The Zircaloy air oxidation model in MELCOR was extended to accommodate the lower anticipated initial cladding temperatures encountered in this analysis. In the calculation of the rate constants and coefficients for oxidation of Zircaloy by oxygen, parabolic kinetics are assumed. Rate constants for air and oxygen reactions with zirconium from a variety of sources were used by Powers et al (1994) in the development of the correlations shown in Figure 4.8 and used in this study. The curves and correlations shown in Figure 4.8 are formulated to describe oxide layer growth. While MELCOR uses an equivalent formulation that describes metal consumed in the reaction. For ZrO_2 creation, 1 (mg $O_2/cm^2)^2$ corresponds to consumption of 8.1274×10^{-4} (kg $Zr/m^2)^2$. Equation 6 lists the modified system of equations employed in MELCOR for the temperature regime of interest. The expressions are interpolated between 1333 and 1550 K.

$$K(T) = \begin{cases} 10.5e^{\frac{-15630}{T}} \left(\frac{kgZr}{m^2}\right)^2 \Big/ s, & T \le 1333K \\ 50.4e^{\frac{-14630}{T}} \left(\frac{kgZr}{m^2}\right)^2 \Big/ s, & T \ge 1550K \end{cases} \qquad (6)$$

Several available correlations are graphically depicted in Figure 4.8. The solid line represents a correlation from Whitehead et al. (1991), the dashed line is from NUREG-1410 (1990). For comparison, the curve marked "steam" is a correlation of parabolic rate constants for steam oxidation of zirconium from Alpert et al. (1988). It is not of any consequence in the present study.

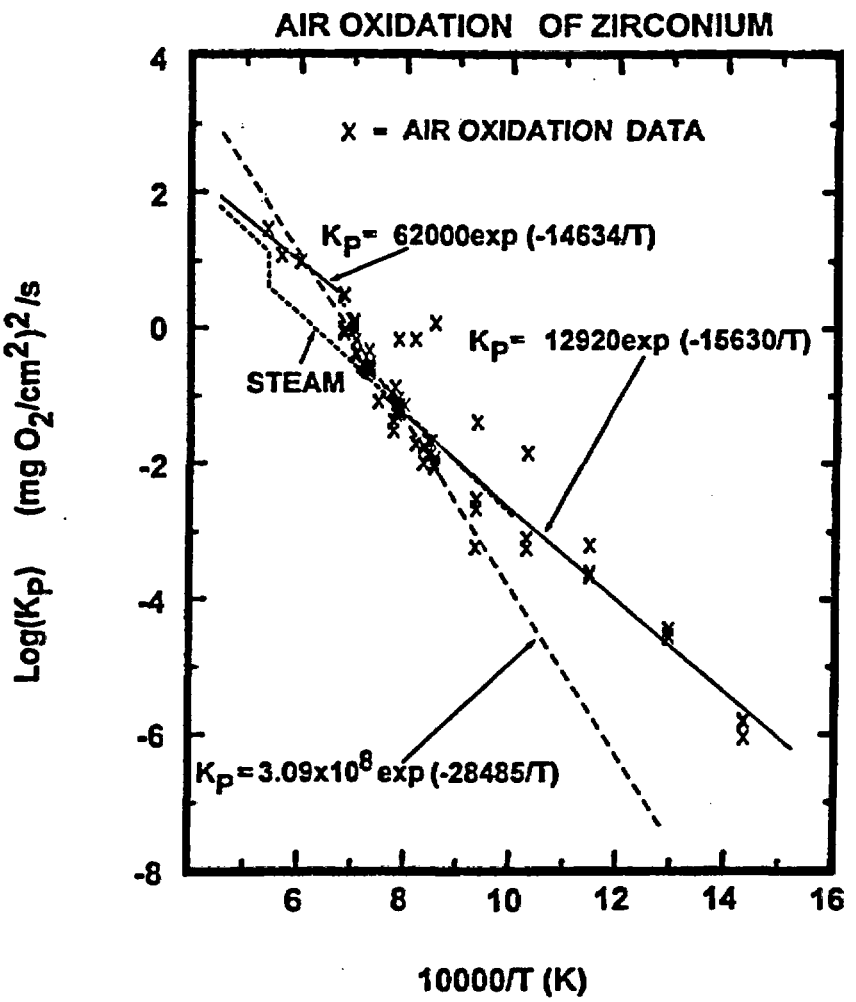

Figure 4.8. Parabolic rate constants for the air oxidation of zirconium.

Model parameters for the Zircaloy oxidation rate constant coefficients modified in MELCOR are listed in Table 4.3. These values are encoded in sensitivity coefficient array 1001. Default minimum and maximum oxidation temperatures are 1100 and 9900 K, respectively. The oxidation cutoff temperature was modified in this study such that Zircaloy oxidation is considered when temperatures exceed 600K. Sensitivity coefficient array 1004 contains this user input.

Table 4.3. Zircaloy oxidation rate constant coefficients, oxidation by O_2.

	Old value	New value
Low temperature range constant coefficient	50.4	10.448
Low temperature range exponential constant	14630	15630
High temperature range constant coefficient	0	50.4
High temperature range exponential constant	0	14630
Upper temperature boundary for low temperature range	10000	1333
Low temperature boundary for high temperature range	10000	1550

These modifications were implemented to better represent air oxidation at low temperatures depicted in Figure 4.8 where 10000/T is in the range of 10 to 16. The default MELCOR coefficients reflected only the higher rate kinetics associated with high temperature oxidation.

MPC Wall Ruptured under otherwise Normal Operating Conditions. The following analysis examines the response of the MPC to an assumed rupture of the outer wall. In this case it is assumed that an axial rip has formed in the wall and is represented by two holes in the upper and lower axial wall sections. Several sensitivities are explored including hole size and oxidation kinetics parameters.

In the first case explored, the holes are assumed to be each 5 cm in diameter. Beginning from a normal operating steady state condition, upon opening the MPC holes at 24 hours, the helium pressurized. The MPC first blows down the helium to the external environment whereupon air promptly replaces the helium. Cool air enters the lower MPC rupture hole and while internal circulation occurs, heated air exits the upper hole. This combination of internal and external air circulation results in a net cool down of the MPC fuel as shown in Figure 4.9.

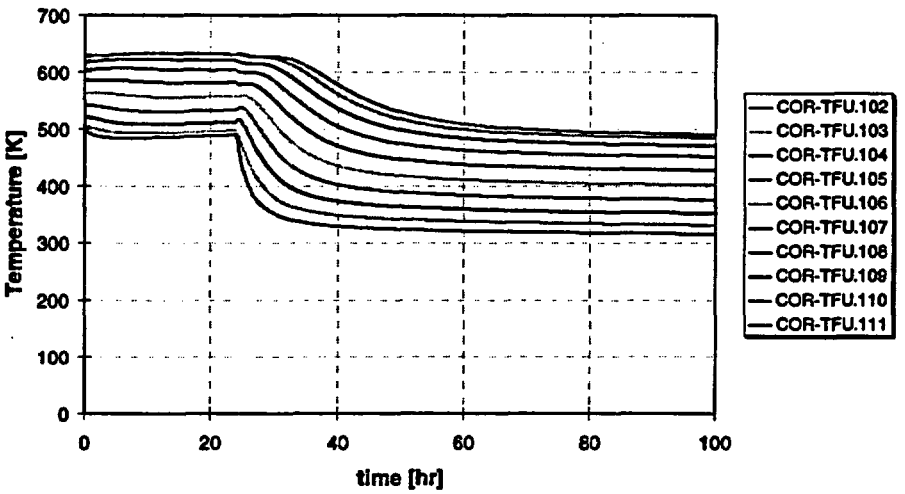

Figure 4.9. Ring 1 fuel response to air ingression from normal initial conditions: two 5 cm diameter holes, default MELCOR oxidation model.

An important element in the cool down shown in Figure 4.9 is the convection of heat out of the MPC by the external circulation pattern, since reducing this convection flow rate by assuming smaller holes (1.6 cm diameter) results in fuel heating instead as shown in Figure 4.10. In this case the holes were opened at time zero and while the lower portions of the fuel assemblies were cooled somewhat, the upper regions began to heat.

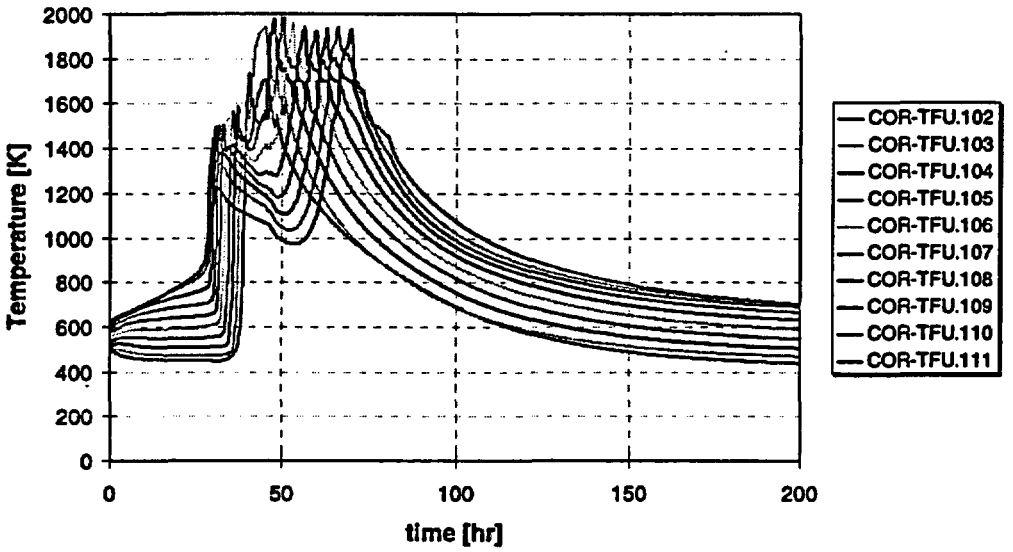

Figure 4.10. Ring 1 fuel response to air ingression from normal initial condition, two 1.6 cm diameter holes, default MELCOR oxidation model.

In this case, using the default MELCOR air oxidation kinetics, as temperatures in the upper portions of the fuel exceed 800K the heat produced by oxidation greatly accelerates subsequent fuel heat-up resulting in the thermal transient at around 30 hours. The transient results from Zircaloy burning in air initiating at the top of the fuel assemblies. In time the burn front of this oxidation transient moves downward toward the source of up-flowing air, starving the upper burning regions of oxidant. When the burn front reaches the bottom of the fuel assembly and consumes available Zr-metal oxygen is again allowed to flow into the upper bundle regions again, resulting in a second burn front migration. This time moving from the bottom of the assemblies, upward resulting slightly slower escalations that reach higher peak temperatures. The entire transient takes place over a period of about 50 hours after which gradual cool down takes place. The Zr-metal is largely converted to ZrO_2 in this process.

The power produced by the air oxidation is shown in Figure 4.11. Initially, only a small amount of heat is produced as air enters the MPC, but as the fuel cladding heats to over 800K, partly due to the small amount of oxidation heating, and partly due to the decreased heat rejection by the low pressure, lower conductivity circulating air, the oxidation kinetic rapidly increase, ultimately producing on the order of 250 kW for about 50 hours. Significant release of fission products to the environment results from this scenario.

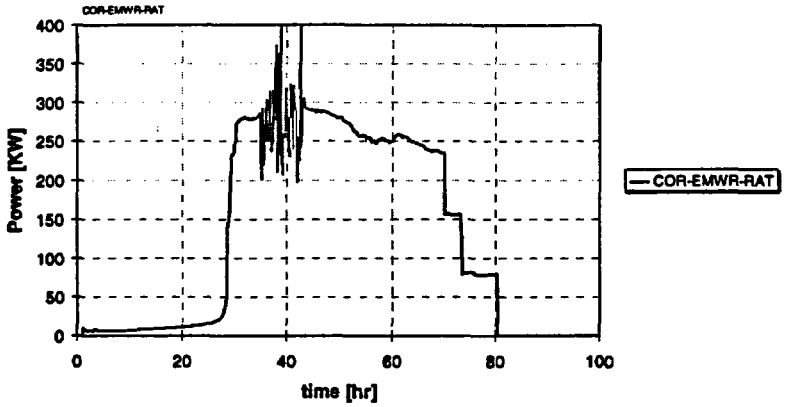

Figure 4.11. Air oxidation power in MPC, default MELCOR oxidation model.

In view of the results shown in figures 4.9, 4.10, and 4.11, indicating the relative ease by which severe fuel damage conditions can be attained, we subsequently explored more closely the nature of the air oxidation kinetics in use. This review revealed that the default air oxidation kinetics in use in MELCOR is more appropriate for oxidation at higher temperatures (i.e., ≥ 1400 K), but likely overestimate the oxidation rate in the 600 to 800 K range important in this analysis. The review of air oxidation models by Powers summarized in Figure 4.8 provides rate coefficients more appropriate for this low temperature oxidation regime. This was used in this and subsequent analyses producing the fuel heat-up response shown in Figure 4.12. In this case, again heating is observed in the upper fuel assembly regions owing to the comparatively poorer heat transfer properties of the 1-atm circulating air compared to the 5-atm circulating helium in the normally operating MPC.

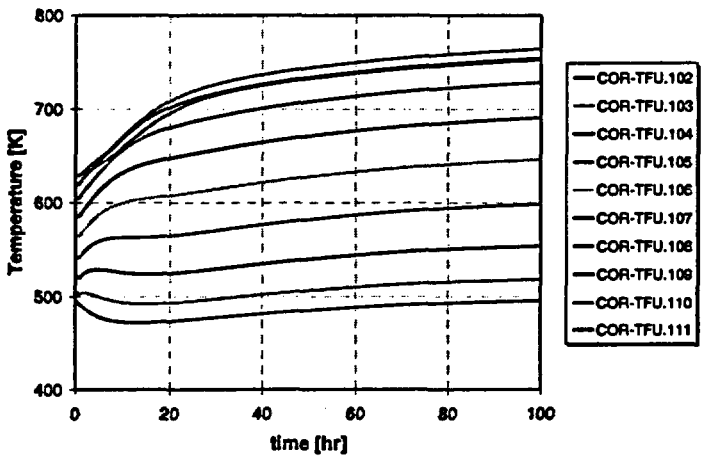

Figure 4.12. Ring 1 fuel response to air ingression from normal initial conditions, two 1.6 cm diameter holes, Powers oxidation model.

Using the revised low temperature air oxidation kinetics results in lower predicted oxidation rates and a lower fuel heat-up rate. Oxidation power for this case is shown in Figure 4.13. The occasional spikes in oxidation power are assumed to be a nodalization effect where different axial fuel zones successively reach temperatures where oxidation initiates. In this case, an oxidation transient resulting in severe fuel damage is averted.

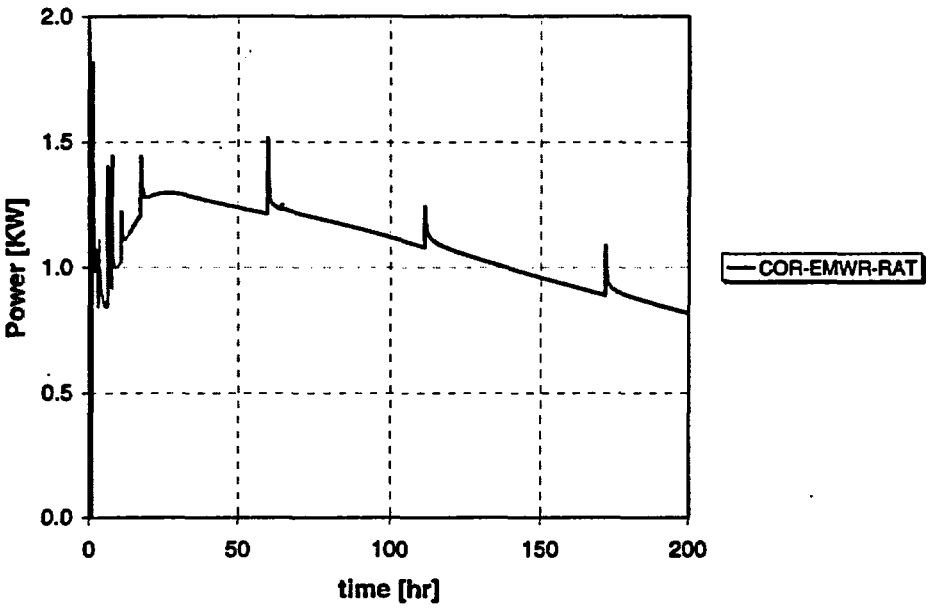

Figure 4.13. Air oxidation power in MPC, Powers oxidation model.

To the extent that the air oxidation models are appropriate in these analyses, it appears that an air oxidation transient initiating from an MPC under normal operating conditions will likely not result in severe damage and large fission product release are not suggested. The following analysis explores the effect of introduction of air to the MPC under off-normal conditions where the over-pack air vents have been blocked prior to the presumed MPC rupture. Presented first is the thermal response of the MPC to vent blocking.

Blocked Over-pack Air Vents. The following analysis presents the thermal response of the MPC to a complete blockage of the over-pack air-cooling vents. Following the steady-state normal operating condition, the inlet and outlet over-pack air-cooling ducts were blocked at 1000 hours. The MELCOR model was permitted to reach a new equilibrium. As expected, fuel temperatures rose in response to total over-pack air vent blockage. Figures 4.14 and 4.15 show that maximum system temperature reached 788K with a corresponding pressure of 6.76 atmospheres. As illustrated in Figure 4.16, mid-height temperatures also reached new equilibrium values. The MPC wall temperature increased from 470K to 643.6K; the over-pack inner wall temperature rose from 345K to 553.7K; and the over-pack outer wall temperature climbed from 313K to 371.7K.

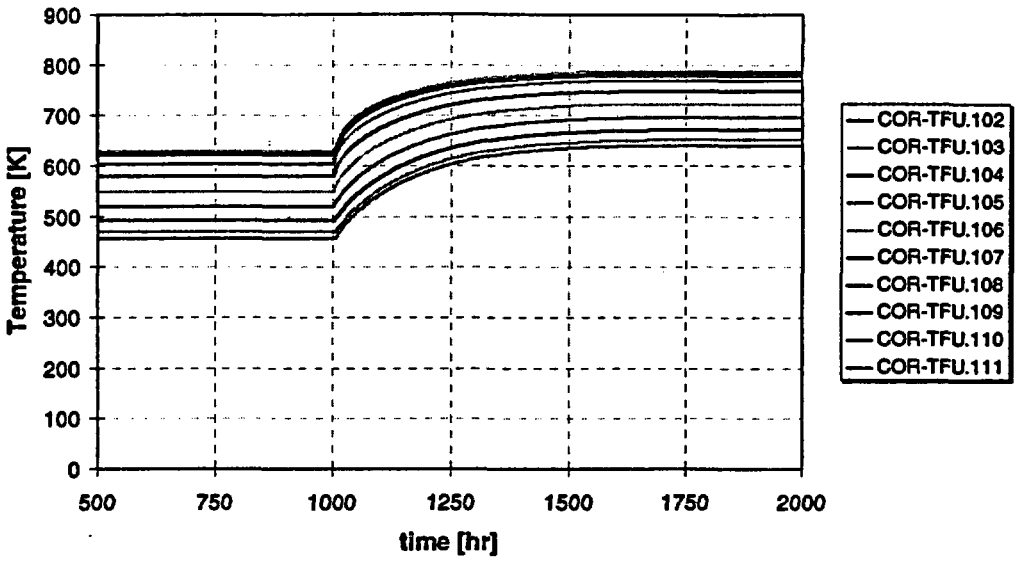

Figure 4.14. Ring 1 fuel temperatures in response to blocked over-pack air vents.

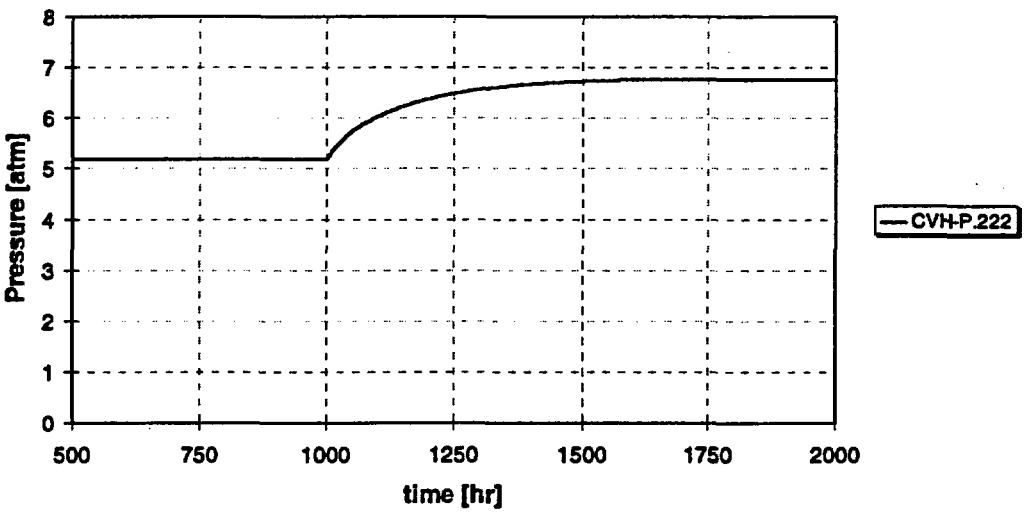

Figure 4.15. MPC pressure response to blocked over-pack air vents.

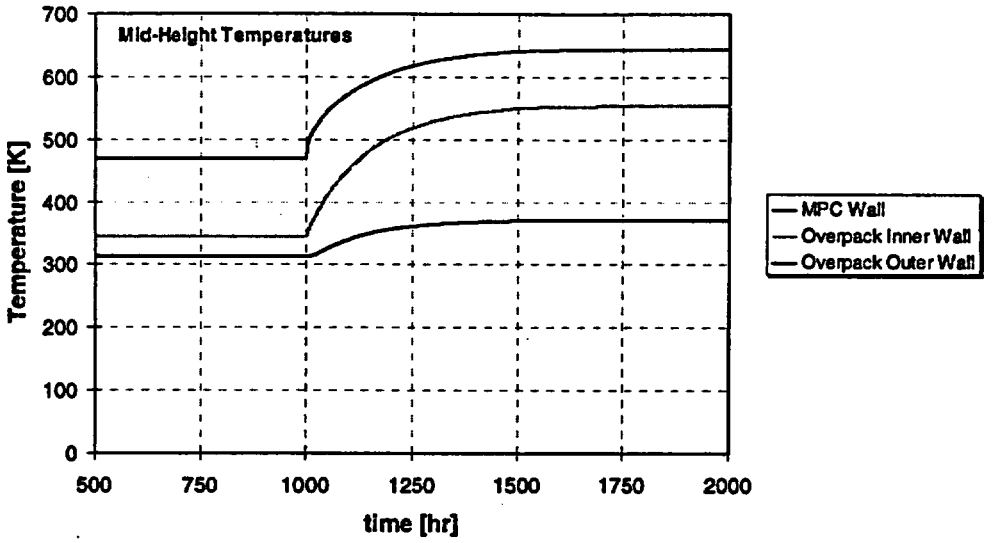

Figure 16. MPC and Over-pack response at mid-height to blocked air vents.

The "cooling duct blockage" accident condition reveals that both the fuel and MPC shell temperatures remain below the short-term temperature limits. However the thermal limit for the concrete over-pack is exceeded. Table 4.4 lists results from the blocked duct thermal transient evaluation reported in the TSAR. The design-basis accident limit pressure listed represents the MPC internal pressure calculated at an ambient temperature of 80°F, 100% fuel rods ruptured, full insolation, maximum decay heat, and at an average temperature of 503.5K. MELCOR results are reported in the last column of Table 4.4.

Table 4.4. Blocked Vents

Parameter	TSAR†	Short-term temperature limits	MELCOR
Temperature, K (°F)			
Fuel Clad	758 (905)	843 (1058)	789
MPC Shell	564 (556)	686 (775)	594
Over-pack Inner Wall	500 (441)	-	554
Over-pack Outer Wall	350 (171)	-	372
Over-pack concrete	-	350 (170)	-
Pressure, atm (psig)	-	7.64 (97.6)	6.77

† TSAR Section 11.2 and13.2, and Table 11.2.9

Analysis presented in the TSAR provided temperatures after 72 hours of duct blockage. The MELCOR analysis proceeded well beyond the 72 hours indicating the TSAR values are not the upper limit. The MELCOR predicted temperatures do not exceed the short-term temperature limits. The predicted over-pack wall temperatures did, however, exceed the short-term temperature limit of 350K.

The following section presents an analysis wherein the MPC wall is ruptured after MPC temperatures have reached the higher equilibrium associated with this blocked vent scenario. As will be shown, clad temperatures in this range are sufficiently high that self-sustaining air oxidation results.

Blocked Vents with MPC Wall Rupture. New equilibrium conditions are established subsequent to air-duct blockage. The MELCOR input deck for the air-ingression scenario was initialized using the equilibrium condition from the aforementioned blocked vent case. Rupturing of the MPC was simulated by the placement of two holes in the MPC wall, one located at the top of the baseplate and the other, four meters above it. The two 1.6 cm diameter penetrations in the MPC wall are opened after one hour of operation at the elevated temperatures induced by the blocked over-pack vents. System pressure and temperature response are depicted in Figure 4.17 and Figure 4.18, respectively. System blow down immediately follows MPC wall rupture. Upon rupture of the MPC wall it is further assumed that the over-packed air ducts become cleared, allowing air to enter the cooling annulus. Air ingress into this initially inert system through the apertures precipitates a dramatic temperature transient. In this case, the Powers oxidation parameters appropriate for low temperature oxidation were employed.

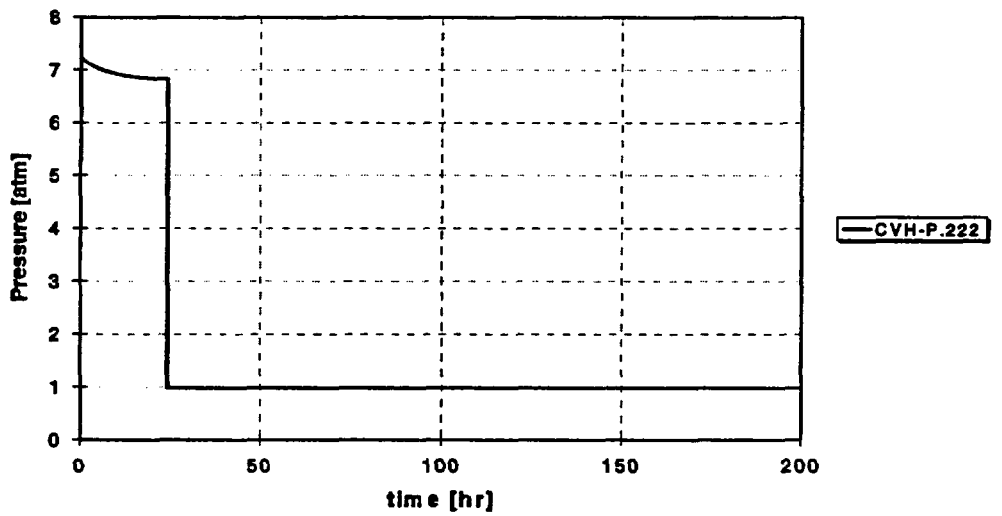

Figure 4.17. MPC pressure response to blocked over-pack air vents for a ruptured cask.

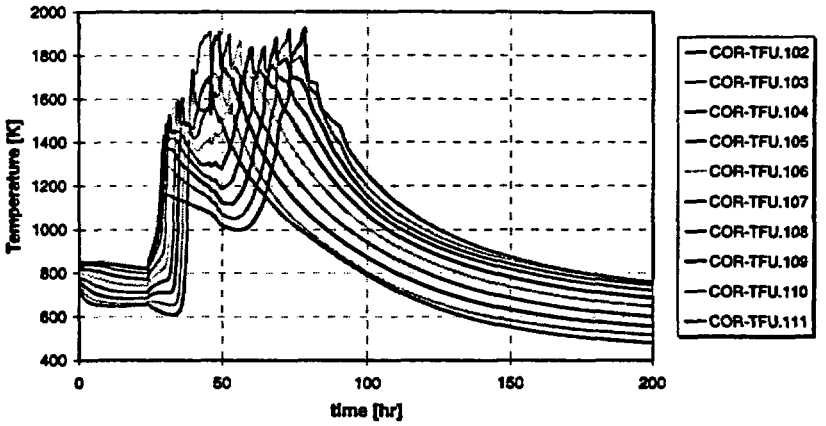

Figure 4.18. Ring 1 fuel response to blocked vents following air ingress through two 1.6 cm diameter holes (Powers oxidation model).

The introduction of air into the MPC, thus heated by previously blocked air vents, leads to ignition of a self-sustaining air oxidation reaction. Again, the reaction begins at the top of the fuel assemblies and migrates downward toward the source of up-flowing air, starving downstream cladding of oxygen. After reaching the bottom of the assembly, the oxidation front reverses direction and proceeds back upwards toward the top of the assembly, consuming the metal not oxidized by the initial downward-moving burn front. This first downward and then upward movement of the oxidation front is reflected in the growth characteristics of the cladding oxide layer as shown in Figure 4.19. Figure 4.20 shows the oxidation power produced during the transient, which occurs over a period of about 50 hr and reaching peak temperatures on the order of 1800K.

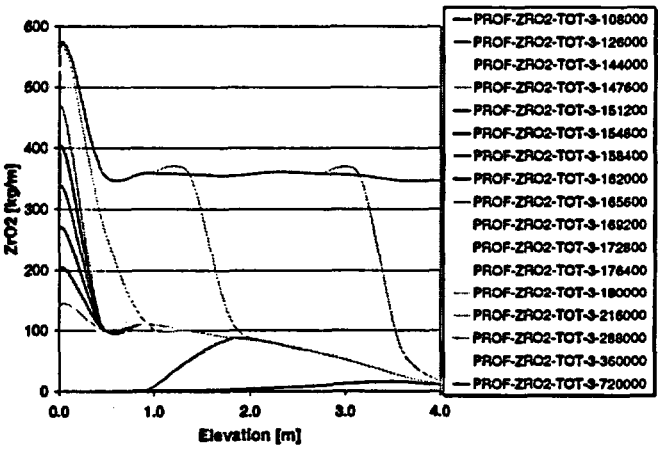

Figure 4.19. Axial and temporal profile of ZrO2(Powers oxidation model).

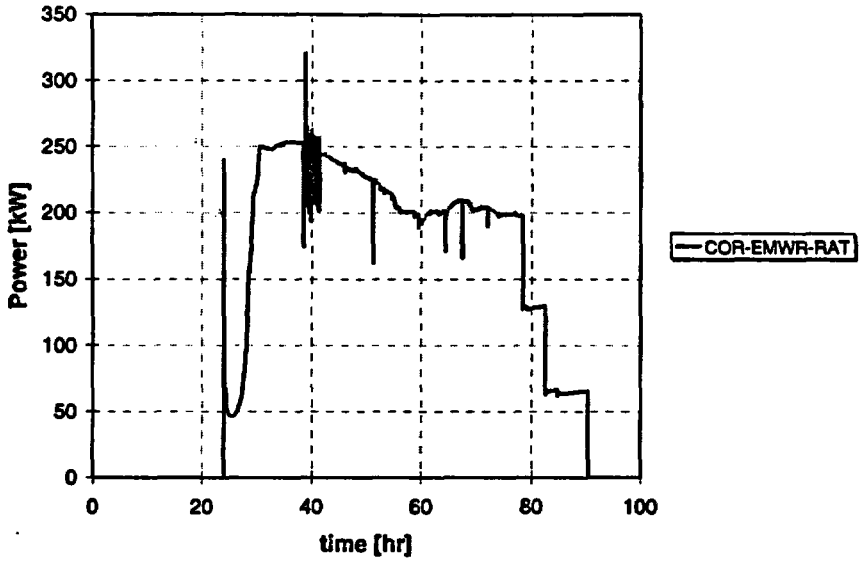

Figure 4.20. Air oxidation power in MPC (Powers oxidation model).

While gross collapse of the fuel assemblies would not likely result from these temperatures, extensive fission product release from the damaged fuel is predicted. Predicted releases of noble gas and Cs are shown in Figure 4.21 and Figure 4.22. Noble gas environmental release is nearly 80%, and cesium release to the environment is just over 70%, with 10% retained within the MPC. Table A2 lists the classes of radionuclides evaluated in MELCOR and the quantities released in the current model.

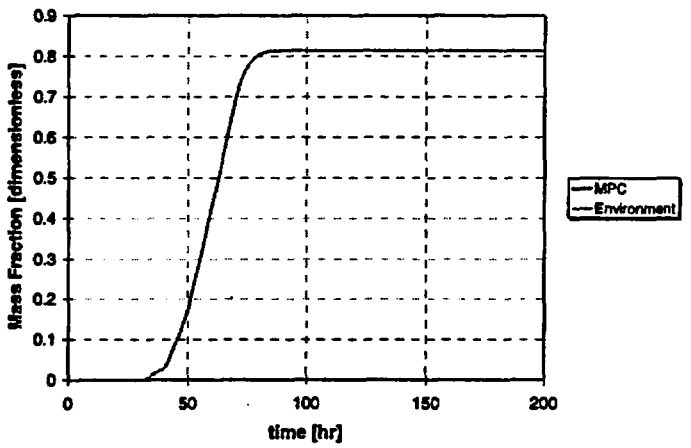

Figure 4.21. Noble gas released to environment during air oxidation transient.

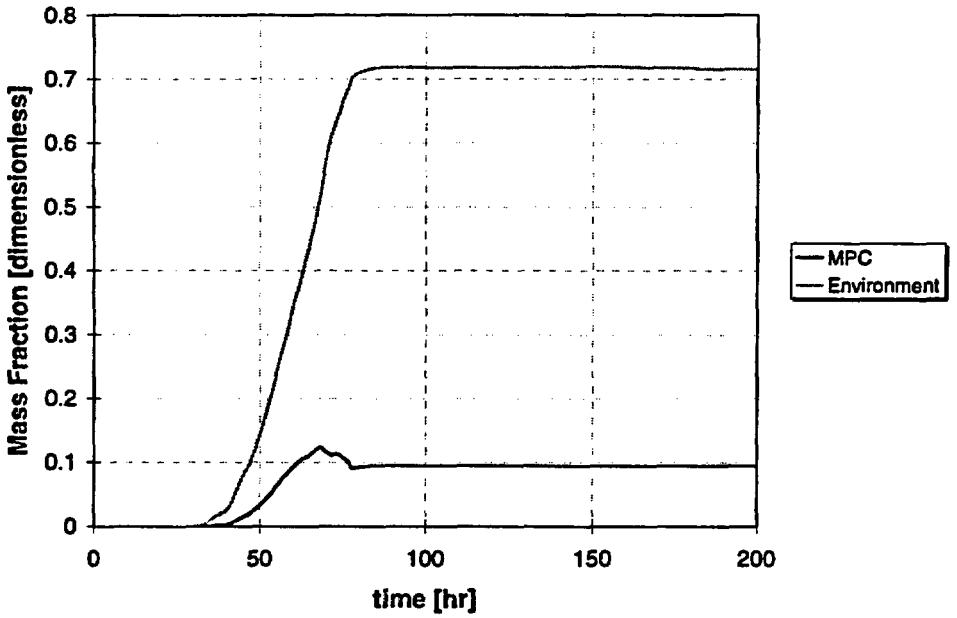

Figure 4.22. Cesium released to environment during air oxidation transient.

An Analytical Experiment: Response of Air-filled system. In order to gain greater insight into the factors operative in the fuel heat-up following MPC rupture and air ingress, the following "analytical experiment" was performed. In this experiment, the MPC temperatures were initialized at time zero with temperatures associated with steady-state operation under normal conditions (i.e., with the MPC filled with 5 atm Helium). Air was then "instantly" substituted for the normal He fill gas, and the Zircaloy air oxidation model was suppressed. This meant that the observed thermal response was that caused only by heat transfer through the thermal working fluid. The change in fuel temperatures when air instead of helium is present thus shows the effect of changing gas properties from those of helium to those of air. Figure 4.23 shows that for the first 100 hrs of this analysis, most of the fuel heats up somewhat owing to the fact that the circulating air is less effective in transferring heat to the MPC wall and therefore enters the bottom of the fuel assemblies at a higher temperature than when helium was present. Figure 4.24 shows that at 100 hrs, the system was allowed to depressurize to one atm and Figure 4.25 shows that at this time external air exchange was artificially surpressed. Figure 4.23 also shows that the loss of mass in the circulating fluid at 100 hrs caused by depressurization to one atmosphere caused an even larger heat-up of the MPC fuel. These results show that fuel heating occurs for two reasons when air replaces helium as the working fluid: 1) the lower thermal conductivity of air relative to helium results in lower heat transfer properties and 2) lower working fluid pressure (i.e., fewer moles of gas) limits the amount of heat that can be removed from the fuel. Both of these effects can facilitate the ignition of Zircaloy oxidation with by air.

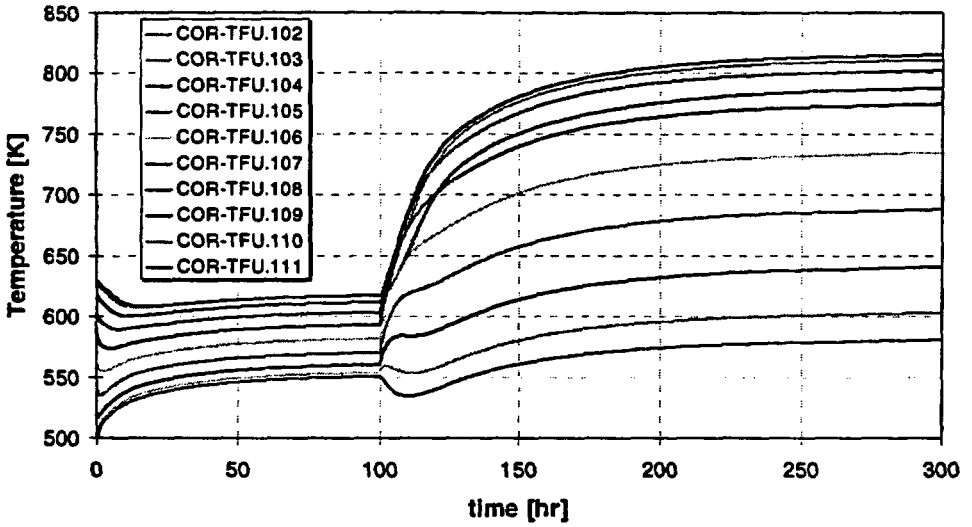

Figure 4.23. Temperatures resulting from replacing helium with air starting from normal operating temperatures followed by blow down to 1 atm at 100 hr.

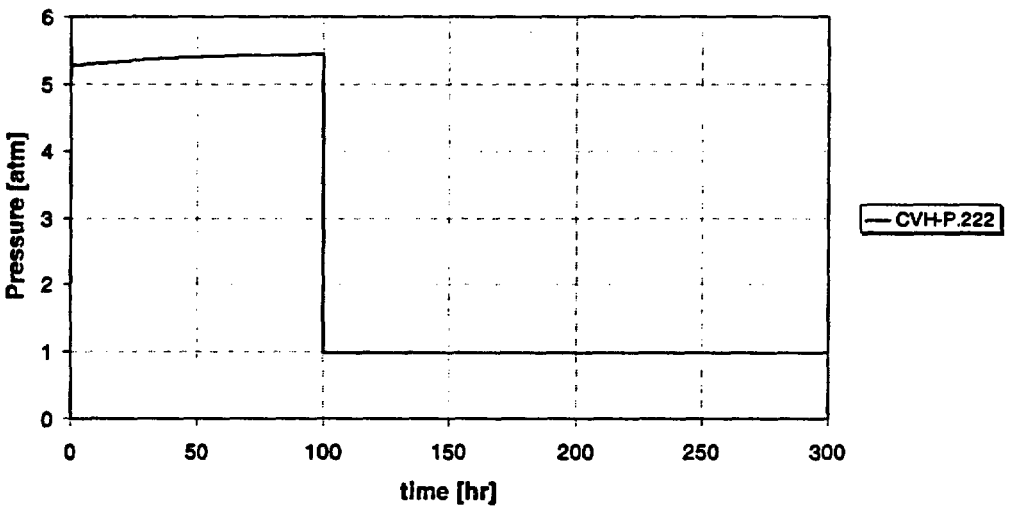

Figure 4.24. Pressure resulting from replacing helium with air starting from normal operating temperatures followed by blowdown to 1 atm at 100 hr.